Contents lists available at ScienceDirect

Bioactive Materials

Prophylaxis of posterior capsule opacification through autophagy activation with indomethacin-eluting intraocular lens

Xiaobo Zhang [a,b,1], Jing Wang [c,1], Jingwei Xu [a,1], Wen Xu [a,b], Yin Zhang [b], Chenqi Luo [a,b], Shuang Ni [a], Haijie Han [a,b,**], Xingchao Shentu [a,b], Juan Ye [a,b], Jian Ji [c,*], Ke Yao [a,b,***]

[a] Eye Center, The Second Affiliated Hospital, School of Medicine, Zhejiang University, Hangzhou, 310009, PR China
[b] Zhejiang Provincial Key Lab of Ophthalmology, The Second Affiliated Hospital, School of Medicine, Zhejiang University, Hangzhou, 310009, PR China
[c] MOE Key Laboratory of Macromolecule Synthesis and Functionalization of Ministry of Education, Department of Polymer Science and Engineering, Zhejiang University, Hangzhou, 310027, PR China

ARTICLE INFO

ABSTRACT

Posterior capsule opacification (PCO) is the most common long-term postoperative complication of cataract surgery, leading to secondary vision loss. Optimized intraocular lens (IOL) structure and appropriate pharmacological intervention, which provides physical barriers and biological inhibition, respectively, can block the migration, proliferation, and epithelial-mesenchymal transition (EMT) of lens epithelial cells (LECs) for PCO prophylaxis. Herein, a novel indomethacin-eluting IOL (INDOM-IOL) with an optimized sharper edge and a sustained drug release behavior was developed for PCO prevention. Indomethacin (INDOM), an ophthalmic non-steroidal anti-inflammatory drug (NSAID) used for postoperative ocular inflammation, was demonstrated to not only be able to suppress cell migration and down-regulate the expression of cyclooxygenase-2 (COX-2) and EMT markers, including alpha-smooth muscle actin (α-SMA) and cyclin D1, but also promote the autophagy activation in LECs. Additionally, autophagy was also verified to be a potential therapeutic target for the down-regulation of EMT in LECs. The novel IOL, serving as a drug delivery platform, could carry an adjustable dose of hydrophobic indomethacin with sustained drug release ability for more than 28 days. In the rabbit PCO model, the indomethacin-eluting IOL showed excellent anti-inflammatory and anti-PCO effects. In summary, indomethacin is an effective pharmacological intervention in PCO prophylaxis, and the novel IOL we developed prevented PCO *in vivo* under its sustained indomethacin release property, which provided a promising approach for PCO prophylaxis in clinical application.

1. Introduction

To date, cataract is still the primary cause of impaired vision in the world. Phacoemulsification surgery is the most commonly effective treatment strategy [1,2]. However, posterior capsule opacification (PCO) after surgery can lead to secondary vision loss, despite the success of the surgery [3]. PCO occurs in 20–40% of adult surgical patients within the first two years after surgery, and the incidence reaches almost 100% in pediatric patients [4]. PCO also has a more serious impact on the low-income and uninsured patients living in developing counties due to the extra economic burden. Therefore, it is vital to explore a safe and effective prophylactic strategy for PCO.

PCO is a wound-healing response after surgery, which results from the migration and proliferation of the surviving lens epithelial cells (LECs) into the posterior capsule [5]. Currently, neodymium-doped yttrium aluminum garnet (Nd: YAG) laser therapy is the only effective strategy when PCO occurs; however, this treatment still has various risks, including intraocular lens (IOL) damage, cystoid macular edema, uveitis, glaucoma, and retinal detachment [6,7]. Therefore, studies on PCO mainly focused on exploring prophylactic strategies, especially

including the redesign and modification of IOLs. IOLs with sharper edges were verified to be more effective in reducing the incidence of PCO [8]. Alternatively, the IOLs were surface-modified by heparin, polyethylene glycol (PEG), and phosphorylcholine to inhibit PCO by reducing cell adhesion [9–11]. Recently, various kinds of drugs, especially anti-proliferative drugs, such as disulfiram, methotrexate, and doxorubicin, were loaded on IOLs as drug delivery platforms for directly killing residual LECs for PCO prevention [12–14]. However, the toxic drugs loading on IOLs carried the risk of corneal epitheliopathy, maculopathy, and dysfunctional tear syndrome, limiting their further clinical application [15].

During the development of PCO, the migration, proliferation, and fibrosis of LECs are associated with epithelial-mesenchymal transition (EMT) [4,16]. Studies have shown that several cytokines with elevated concentrations in postoperative aqueous humor stimulated the EMT process of LECs [17–19]. Arnaud et al. found that postoperative intraocular inflammation and PCO formation were related to the tumor necrosis factor-alpha (TNF-α) with a high concentration in aqueous humor, which could even be considered as a predictor of PCO [20]. It is reported that cyclooxygenase-2 (COX-2) and prostaglandin had high expression levels in clinical specimens of PCO, and COX-2 inhibitors have also been shown to repress PCO formation *in vivo* [21]. However, the role of COX-2 during the development of PCO remains unknown. Autophagy is known as an evolutionarily conserved process for cellular homeostasis maintenance, and it exerts self-degradation or self-protection according to the different conditions [22–25]. Previous studies demonstrated that cyclosporine A and rapamycin had the potential to suppress PCO by mediating autophagy in LECs [26,27]. Although these drugs also present risks to intraocular tissues, it sheds new light on the choice for anti-PCO medicines. In addition, whether there is an interaction between autophagy and EMT needs further investigation. Indomethacin (INDOM), an ophthalmic non-steroidal anti-inflammatory drug (NSAID), is an effective inhibitor of cyclooxygenase (COX), especially on COX-2 [28–30]. Recent studies found that INDOM was capable of activating autophagy [31,32], which provides a more promising possibility for the growth inhibition of LECs, so as to prevent PCO. However, the bioavailability of ophthalmic drugs in ocular tissue through topical administration is limited to 3% by the corneal epithelial barrier [33,34], and the

hydrophobic INDOM is more difficult to affect the posterior capsule for PCO prevention through topical eye drops.

In this study, we designed and constructed an INDOM-eluting IOL (INDOM-IOL) based on ultrasonic spray technology. Degradable poly (lactic-co-glycolic acid) (PLGA) was adopted as the coating to release INDOM in the lens capsule directly and continuously for PCO prevention (Scheme 1). The safety and drug release properties of the novel IOL were evaluated scrupulously. Moreover, we investigated the effect of INDOM on EMT and the autophagy-mediated migration and proliferation in LECs, and established a rabbit PCO model to assess the prophylactic effect of the INDOM-IOL. This work demonstrated the efficacy of INDOM-IOL as a pharmacological intervention and brought a promising strategy for PCO prevention in clinic.

2. Material and methods

2.1. Materials and reagents

INDOM and ophthalmic 0.5% INDOM in castor oil solution was obtained from Senju Pharmaceutical Co. Ltd. (Osaka, Japan). Hydrophobic acrylic IOLs with plate haptics were customized from Wuxi Vision Pro Ltd. (Wuxi, China). PLGA (lactide: glycolide 75:25, Mw: 40,000–75,000) was purchased from Sigma Chemical Co. (St. Louis, MO, USA). Recombinant human TNF-α was obtained from PeproTech, Inc. (Cranbury, NJ, USA). 3-Methyladenine (3-MA) was obtained from MedChemExpress LLC. (Shanghai, China). Dulbecco's Modified Eagle Medium: Nutrient Mixture F-12 (DMEM/F12), 0.25% trypsin with 0.02% ethylene diamine tetraacetic acid (EDTA), Lipofectamine 2000 reagent, Opti-MEM, and fetal bovine serum (FBS), were purchased from Thermo Fisher Scientific (Carlsbad, CA, USA). Cell counting kit-8 (CCK-8) was obtained from Dojindo Laboratories (Kumamoto, Japan). Calcein-AM/PI double stain kit was obtained from Yeasen Biotech Co., Ltd. (Shanghai, China).

2.2. Preparation of drug-eluting IOLs

The hydrophobic acrylic IOLs with plate haptics were used as drug delivery platforms. The PLGA (5 wt %) and INDOM in ethyl acetate
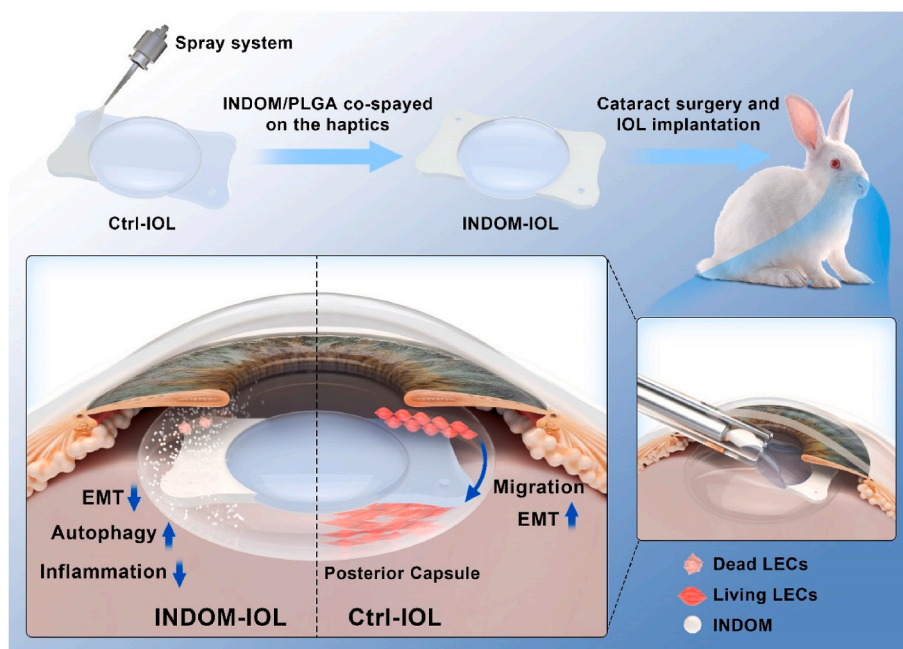
Scheme 1. Schematic illustration of INDOM-IOL as a prophylactic strategy for PCO. INDOM could not only inhibit migration and EMT, but stimulate the activation of autophagy in LECs as well. INDOM-IOL was prepared as a drug delivery platform with INDOM/PLGA co-sprayed on the plate haptics. The prophylactic effect of the INDOM-IOL on PCO was confirmed in a rabbit PCO model.

solution were sprayed on the plate haptics of IOLs using an ultrasonic coating system (Shanghai Ruidu Photoelectric Co., Ltd, Shanghai, China) [35,36]. The coating was only sprayed on the haptics of IOLs, which ensured the smoothness and transparency of IOLs. Three kinds of IOLs were prepared and established in the present study: 1) control-IOL (Ctrl-IOL) = IOL without any treatment; 2) PLGA-IOL = IOL with PLGA sprayed; 3) INDOM-IOL = IOL with PLGA and INDOM sprayed. Each INDOM-IOL carried approximately 100 μg of INDOM. All IOLs were sterilized with exposure to ethylene oxide before being used in animal experiments.

2.3. Drug-release kinetics and surface characterization of drug-eluting IOLs

The water contact angle of the hydrophobic IOL surface was evaluated with a Kruss DSA 100 system (Hamburg, Germany) to assess the surface wettability. The transmittance of the IOL optical center was measured by an Evolution 300 ultraviolet–visible spectrometer (UV–vis; Thermo Scientific, Carlsbad, CA, USA). The morphology and thickness of the coating on IOLs were observed by scanning electron microscopy (SEM; Hitachi S4800, Tokyo, Japan).

The UV–vis spectrometer was used to detect the drug release profile of INDOM-IOLs in a phosphate-buffered saline (PBS) medium. Firstly, we use the UV–vis spectrometer to detect the absorbance value of the standard INDOM in PBS with different concentrations at 320 nm, and the standard curve of INDOM was obtained accordingly. Next, each INDOM-IOL was placed in a prepared tube which was filled with 10 mL PBS, and the IOL was wholly immersed in the solution. Afterward, the tube was incubated at 37 °C in a thermostated container with continuously shaken (100 rpm). Subsequently, 4 mL of the solution in the tube was taken out and replaced with 4 mL fresh PBS medium at predetermined time points. The absorbance value of the removed media was measured by the UV–vis spectrometer. Then, based on the standard curve we have established above, the concentrations of INDOM in the solution were figured out, and the release curve of INDOM was obtained through the repeated experiments.

2.4. Cell culture and animals

Three cell lines were involved in the present study, including human lens epithelial cell line (HLEC-B3), human corneal epithelial cells line (HCEC), and human retinal pigment epithelial cell line (ARPE-19). The cell lines were acquired from the American Type Culture Collection (ATCC, Manassas, VA, US) and cultured in DMEM/F12 with 15% FBS, incubated in a 5% CO2 humidified atmosphere at 37 °C, and passaged with 0.25% trypsin-EDTA every two days.

Forty three-month-old Japanese white rabbits (female, bodyweight from 2.0 to 2.5 kg) were obtained from the Zhejiang Academy of Medical Sciences. All animals were handled in accordance with the ARVO Statement for the Use of Animals in Ophthalmic and Vision Research, and all animal experiments were approved by the Laboratory Animal Ethics Committee of the Second Affiliated Hospital, School of Medicine, Zhejiang University (approval No. 098/2022). The animals were randomly divided into four groups (n = 10), which are: 1) Ctrl-IOL group = the right eye was implanted with a Ctrl-IOL; 2) PLGA-IOL group = the right eye was implanted with a PLGA-IOL; 3) Ctrl-IOL with INDOM eye drops (INDOM drops) group = the right eye was implanted with a Ctrl-IOL and received 0.5% INDOM through topical route four times per day for 28 days postoperatively; 4) INDOM-IOL group = the right eye was implanted with an INDOM-IOL.

2.5. Transwell migration assay

The LECs were seeded in the *trans*-well chamber (Merck Millipore) 200 μL serum-free DMEM/F12 medium, while the compartment between the chamber and 24-well plates was added with 600 μL DMEM/ F12 with 15% FBS. Afterward, the LECs were fixed in 4% paraformaldehyde (PFA) for 15min. Next, the cells were stained with 0.3% crystal violet after 24 h of incubation. The images were captured with a Leica phase-contrast microscopy (Wetzlar, Germany).

2.6. Wound-healing assay

The LECs were seeded in 6-well plates and incubated for 24 h. The LECs were divided into four groups: 1) control group = LECs without treatment; 2) TNF-α group = LECs were treated with TNF-α (10 ng/mL) alone; 3) TNF-α + 100 INDOM group = LECs treated with TNF-α (10 ng/mL) and 100 μM INDOM; 4) TNF-α + 300 INDOM group = LECs treated with TNF-α (10 ng/mL) and 300 μM INDOM. After being treated with INDOM for 2 h, the LECs were triggered by TNF-α (10 ng/mL). Then, the wounds were generated with a 1 mL sterile pipette tip. The images were captured with microscopy (Olympus, Tokyo, Japan) at 0 h and 24 h after wound generation.

2.7. Western blot analysis

The treated LECs were harvested and lysed from 6 cm culture dishes with lysis buffer (Sangon, Shanghai, China). A bicinchoninic acid Protein Assay Kit (Thermo Scientific, Carlsbad, CA, USA) and A spectrophotometer (Bio-Rad, CA, USA) were applied in this section for protein concentration detection. Equal proteins from each sample were loaded onto the sodium dodecyl sulfate-polyacrylamide gel electrophoresis (SDS-PAGE), and then transferred onto PVDF membranes. Afterward, immunoblot assay was performed. Antibodies and their dilution ratios were as follows: anti-rabbit LC3 (1:1000; Sigma Aldrich, MO, USA); anti-rabbit Atg5 (1:1000; CST, MA, USA); anti-rabbit Beclin-1 (1:1000; CST, MA, USA); anti-rabbit P62 (1:1000; CST, MA, USA); anti-rabbit COX-2 (1:1000; CST, MA, USA); anti-rabbit alpha-smooth muscle actin (α-SMA; 1: 3000; Abcam, Waltham, MA, USA); anti-rabbit Snail (1: 1000; CST, MA, USA); anti-rabbit GAPDH (1:2000; CST, MA, USA); anti-rabbit β-tubulin (1:2000; CST, MA, USA); anti-mouse cyclin D1 (1:1000; CST, MA, USA); horseradish peroxidase (HRP)-conjugated secondary antibody (1:5000; CST, MA, USA).

2.8. Immunofluorescence assay

The LECs were seeded in 24-well plates with DMEM/F12 containing 15% FBS. The LECs were fixed with 4% PFA for 30 min after treatment. Next, The LECs were permeated with 0.5% Triton X-100 (Sigma Aldrich, MO, USA) for 15 min. Afterward, the cells were blocked with 10% goat serum (Sigma Aldrich, MO, USA) for 1 h. Anti-rabbit LC3 antibody (1:100; Sigma Aldrich, MO, USA), anti-rabbit Snail antibody (1:100; Proteintech, Rosemont, IL, USA), and anti-mouse P62 antibody (1: 100; Abcam, Waltham, MA, USA) were used as primary antibodies. Alexa Fluor 488-conjugated anti-rabbit IgG antibody (1:1000; CST, MA, USA), Alexa Fluor 488-conjugated anti-mouse IgG antibody (1:1000; CST, MA, USA), and Alexa Fluor 555-conjugated anti-rabbit IgG antibody (1:1000; CST, MA, USA) were used as secondary antibodies. Alexa Fluor 555-Phalloidin (1:100, Thermo Fisher Scientific, Carlsbad, CA, USA) was used to stain the F-actin of cells for 45 min. The images were captured with a confocal microscope (Leica TCS SP8, Wetzlar, Germany). In addition, the cells were stained with 100 nM Lysotracker Red (Solarbio, Beijing, China) for 10 min to detect the lysosomes, and the results were captured with a fluorescence microscope (Leica, Wetzlar, Germany).

The tissues from the rabbit eyes were fixed with 4% PFA for 24 h. Afterward, the samples were permeated with 0.5% Triton X-100 (Sigma Aldrich, MO, USA) for 15 min. After being blocked with 10% goat serum, the tissues were incubated with a mouse monoclonal anti-tubulin antibody (1:100; Proteintech, Rosemont, IL, USA) and Alexa Fluor 488-conjugated anti-rabbit IgG secondary antibody. Then, Alexa Fluor 555-Phalloidin (1:100, Thermo Fisher Scientific, Carlsbad, CA, USA) was used to stain the F-actin of the samples for 45 min, and the results were

obtained with a Leica fluorescence microscope (Wetzlar, Germany). All immunofluorescence assays were performed using DAPI (Sigma Aldrich, MO, USA) staining for nuclear localization.

2.9. Transmission electron microscopy (TEM) analysis

The LECs were fixed in 2% glutaraldehyde and 2% PFA in 100 μM phosphate buffer (pH 7.4) at 4 °C for 4 h. Then, the samples were post-fixed with 1% OsO_4 in 100 μM phosphate buffer (pH 7.4) for 2 h. Afterward, the samples were dehydrated gradually and embedded in epon resin, and then cut to 65–70 nm thin sections. The ultrathin sections were examined with TEM (Hitachi HT7800, Tokyo, Japan).

2.10. siRNA transfection

The LECs were seeded in 6-well plates and transfected with 100 pmol of P62 siRNA or negative control (NC) siRNA using Lipofectamine 2000 reagent (Invitrogen, Carlsbad, CA, US) and a reduced serum medium (Opti-MEM, Gibco, Grand Island, NY, US) according to the manufacturer's protocol. The following siRNA sequences were involved in this experiment: P62 siRNA (sense: 5′- GUG ACG AGG AAU UGA CAA UTT - 3′, anti-sense: 5′- AUU GUC AAU UCC UCG UCA CTT - 3′), and NC siRNA (sense: 5′- UUC UCC GAA CGU GUC ACG UTT - 3′, anti-sense: 5′- ACG UGA CAC GUU CGG AGA ATT - 3′). All the siRNAs were synthesized by GenePharma Co. (Shanghai, China). The LECs were divided into different groups as follows: 1) NC siRNA group = NC siRNA transfection only; 2) P62 siRNA group = P62 siRNA transfection only; 3) NC siRNA + TNF-α group = NC siRNA transfection and treated with 10 ng/mL TNF-α; 4) P62 siRNA + TNF-α group = P62 siRNA transfection and treated with 10 ng/mL TNF-α; 5) NC siRNA + TNF-α + INDOM group = NC siRNA transfection and treated with 10 ng/mL TNF-α and 300 μM INDOM; 6) P62 siRNA + TNF-α + INDOM group = P62 siRNA transfection and treated with 10 ng/mL TNF-α and 300 μM INDOM.

2.11. Cell counting kit-8 (CCK-8) assay

The LECs were seeded in 96-well plates with DMEM/F12 containing 15% FBS. After being treated with INDOM in different concentrations for 24 h, the cells were incubated with 10% CCK-8 in PBS solution at 37 °C for 2 h. Finally, the optical density (OD) at 450 nm was measured with an absorbance microplate reader (Bio-Rad iMark, Hercules, CA, USA).

2.12. Live/dead (calcein-AM/PI) double stain test

The LECs were seeded in 24-well plates with DMEM/F12 containing 15% FBS. After being treated with INDOM in different concentrations for 24 h, the LECs were stained with calcein-AM (green) and propidium iodide (PI, red) for 20 min at 37 °C. The results were obtained with a fluorescence microscope (Leica, Wetzlar, Germany).

2.13. IOL implantation experiments in vivo

The right eyes of all rabbits underwent phacoemulsification and intraocular lens implantation. All rabbits were anesthetized with 3% pentobarbital sodium (IV injection, 1 mL/kg of body weight) and dropped with 0.5% tropicamide for pupillary dilation before surgery. All operations were performed by the same surgeon (Dr. Shuang Ni). The primary corneal incision (3.0 mm) and secondary corneal incision (1.0 mm) were made with a keratome. Then, phacoemulsification and IOL implantation were performed with a Bausch & Lomb Stellaris phacoemulsification platform (Bridgewater, NJ, USA). All groups received postoperative topical administration of Pranopulin® (Senju Pharmaceutical Co. Ltd., Osaka, Japan) and Tobradex® (Alcon Laboratories, Inc., USA) four times per day for 14 days. Meanwhile, the rabbits of the INDOM drops group were required an additional 0.5% INDOM topical administration per day for 28 days postoperatively. The right eyes of all

rabbits were evaluated using a slit-lamp camera system (Suzhou 66 Vision-Tech Co. Ltd., Jiangsu, China) at 3 days, 7 days, 14 days, and 42 days after phacoemulsification and IOL implantation surgery, and all the rabbits underwent pupillary dilation with 0.5% tropicamide before being observed. The grading of PCO formation was assessed using retro-illumination images following the previous literature, as shown in Table 1 [37].

All rabbits were sacrificed by overdose anesthesia 42 days after surgery. The sample eyes were fixed with 4% PFA for 24 h. Afterward, the PCO development was further evaluated from the back of the capsule (Miyake-Apple view). The standard hematoxylin and eosin (H&E) staining was performed to observed the ocular tissues, including the corneas, irises, retinas, and posterior capsules. Moreover, the posterior capsules were further assessed using an immunofluorescence assay.

2.14. Statistical analysis

All the data were analyzed with SPSS 23.0 software (SPSS Inc., Chicago, IL, US). The results are presented as means ± standard error of the mean (SEM). Statistical differences were determined using unpaired or paired Student's t-test and one-way ANOVA. A p-value <0.05 was considered significantly different.

3. Results

3.1. Preparation and characterization of INDOM-IOLs

We prepared drug-eluting IOLs, namely INDOM-IOLs, using the custom-made hydrophobic acrylic IOLs with plate haptics and sharp square-edge by ultrasonic spraying equipment, for PCO prevention [38]. In order to avoid impact on optics of IOLs, INDOM and degradable PLGA were uniformly and precisely sprayed on the IOLs' plate haptics. As shown in Fig. 1A, the coating was only sprayed on the plate haptics of IOLs, and the optics remained untreated. The thickness of the coating on the INDOM-IOL was ~6 μm, close to that of the PLGA-IOL, indicating the excellent dispersion of INDOM in PLGA coating (Fig. 1B). UV–vis spectra showed no transparency loss of the IOLs optics since the drug coating only exists on the IOLs' plate haptics (Fig. 1C). The water contact angle of hydrophobic IOLs was measured as 88.7 ± 1.6°. After coating with PLGA or INDOM-PLGA, as shown in Fig. 1D, the water contact angle of the IOLs' coating slightly decreased to 82.3 ± 1.7° or 78.4 ± 1.5°, respectively. The release behaviors of the INDOM-PLGA were evaluated in a PBS medium, which simulated the aqueous humor environment. Of note, approximately 15.3% of the INDOM was released on the first day. 40.7% and 75.7% of the INDOM were released on the 7th day and 28th day, respectively (Fig. 1E). This PLGA-based drug delivery system holds the potential to increase the water solubility of the hydrophobic INDOM, making it more efficient in PCO prevention.

3.2. INDOM inhibited TNF-α-induced migration and EMT in LECs

To investigate the effect of INDOM on migration and EMT in LECs, the cells were treated with INDOM in different concentrations for 24 h. To have a better evaluation, the LECs were triggered by 10 ng/mL TNF-α for another 24 h. The expression of COX-2 and EMT markers, including α-SMA and cyclin D1, were assessed by Western blot. As shown in

Table 1
Grading of PCO formation.

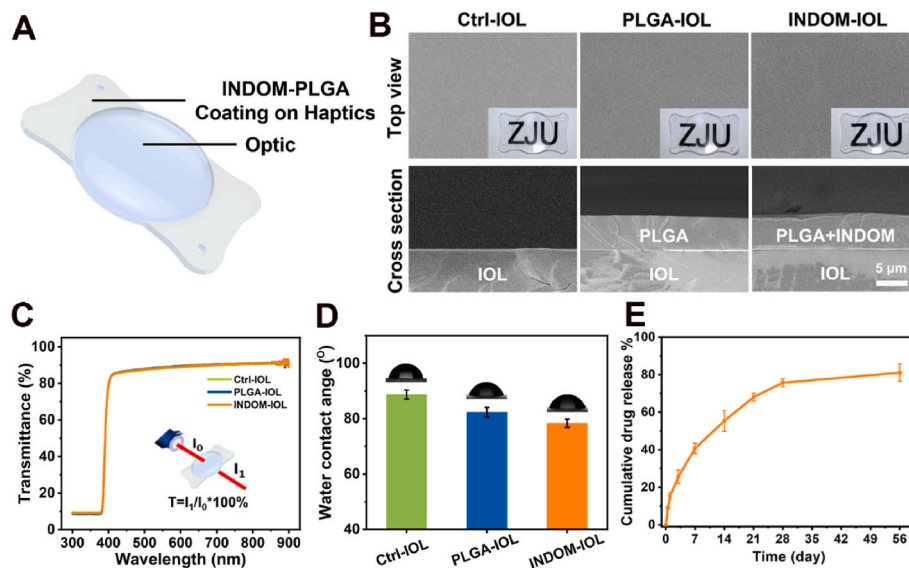| Grades	Severity	PCO formation
0	None	No PCO
1	Slight	PCO not reaching the edge of optic
2	Moderate	PCO reaching the edge
3	Pronounced	PCO beyond the edge but the visual axis is clear
4	Severe	PCO on the visual axis

Fig. 1. Surface characterization of INDOM-IOLs. (A) Schematic diagram of the INDOM-IOL. (B) SEM and bright-field photographs of the three IOLs. SEM pictures exhibited that the coating thickness of INDOM-IOL and PLGA-IOL was ~6 µm (Scale bar, 5 µm). (C) The transmittance of the three IOLs. (D) The water contact angle of the three IOLs. (E) The drug release curve of INDOM-IOLs.

Fig. 2A, B, 2C, and 2D, compared with the TNF-α group, the protein expression levels of COX-2, α-SMA, and cyclin D1 were down-regulated to 0.36 ± 0.03 folds (p = 0.006), 0.33 ± 0.02 folds (p = 0.002), and 0.34 ± 0.03 folds (p = 0.004) by 300 µM INDOM, respectively.

The cell migration capacity was assessed by transwell migration and wound-healing assay. The transwell migration assay showed that the vertical migration ability of the LECs with 10 ng/mL TNF-α treatment was enhanced significantly compared with the control group. Simultaneously, this vertical migration ability was repressed considerably by 300 µM INDOM treatment (Fig. 2E). In the wound-healing assay, after 24 h TNF-α stimulation, similarly, the remaining blank area of the TNF-α group was narrower than that of the group without treatment, indicating that TNF-α significantly promoted cell migration; however, this effect was suppressed by 300 µM INDOM (Fig. 2F). Briefly, these results suggested that INDOM inhibited the migration and EMT of LECs stimulated by TNF-α.

3.3. Activation of autophagy in INDOM-treated LECs

To evaluate the effect of INDOM on autophagy in LECs, we detected the autophagy-related proteins, including Atg5, Beclin-1, P62, and LC3-I/II. Western blot analysis showed that the expression of LC3-II, the activated LC3, significantly increased after exposure to INDOM in a dose-dependent manner, and the relative expression of LC3-II increased to 2.82 ± 0.19 folds (p = 0.016) when treated with 300 µM INDOM for 24 h, compared with the control group (Fig. 3A and F). Similar results were detected in the expression levels of Atg5 and Beclin-1, which also increased after exposure to INDOM in a dose-dependent manner. The expressions of Atg5 and Beclin-1 increased to 3.66 ± 0.21 folds (p = 0.011) and 7.15 ± 0.48 folds (p = 0.009) after being treated with 300 µM INDOM, respectively, compared with the control group (Fig. 3A, C, and 3D). Moreover, the expressions of P62 decreased to 0.19 ± 0.03 folds (p = 0.002) after exposure to 300 µM INDOM compared with the control group (Fig. 3A and E). To further clarify the role of INDOM in autophagy activation, 3-MA, an early-stage autophagy inhibitor, was involved in this study. As shown in Fig. 3B, G, 3H, and 3J, the up-regulation of Atg5, Beclin-1, and LC3-II expressions by 300 µM INDOM were significantly inhibited by 200 µM 3-MA, and similarly, the downregulation of P62 expressions by INDOM was also blocked by 3-MA (Fig. 3B and I). These results indicated that INDOM could significantly promote autophagy activation in LECs.

To further confirm the effect of INDOM on autophagy, immunofluorescence assays were performed. Immunofluorescent images showed that the number of puncta stained with LC3 in the group treated with 300 µM INDOM for 24 h remarkably increased compared with that of the control group (Fig. 4A). Treatment with 300 µM INDOM and 200 µM 3-MA significantly decreased the number of LC3 stained puncta compared with the number in the group treated with INDOM alone. In addition, Lysotracker Red was applied in this section to visualize the autophagy-lysosomes in LECs after staining [39,40]. The enhanced fluorescence signal demonstrated the lysosomal activity in the group treated with INDOM alone, which suggested an activation of autophagy in this group (Fig. 4B). However, in the control group and the group treated with INDOM and 3-MA, few active lysosomes were observed. TEM was used to further observe the autophagy activated by INDOM. The group treated with 1 µM rapamycin (RAPA), an autophagy activator, was introduced as a positive control group in this section. As shown in Fig. 4C, the number of autophagic vacuoles (AV) was increased significantly in both rapamycin (RAPA) group and INDOM group, which indicated the activation of autophagy. To sum up, the above results demonstrated that INDOM effectively stimulated the activation of autophagy in LECs.

3.4. Activation of autophagy suppressed TNF-α-stimulated EMT in LECs

To further investigate the relationship between autophagy and EMT in LECs, the siRNA transfection was used in this study. The function of the specific genes could be elucidated more definitively by knocking down with siRNA transfection. P62 is an essential autophagy substrate, which has a positive regulatory effect on Snail [41]. Snail is known as a critical transcription factor in the process of EMT in LECs [38]. Therefore, the interaction of P62 and Snail was investigated. As shown in Fig. 4, knockdown of P62 by siRNA significantly suppressed Snail expression after TNF-α treatment. Fig. 4D illustrated the mechanism of INDOM inhibiting EMT *via* activation of autophagy in LECs. Compared with the NC siRNA + TNF-α group, 300 µM INDOM showed significant down-regulation of the TNF-α-triggered over-expression of Snail (0.16 ± 0.01 folds, p = 0.006, Fig. 4E and I), α-SMA (0.39 ± 0.06 folds, p = 0.014, Fig. 4E and G), and cyclin D1(0.33 ± 0.05 folds, p = 0.024, Fig. 4E and H). Instead, there were no statistical differences in the expression of Snail (1.07 ± 0.04 folds, p = 0.745, Fig. 4E and I), α-SMA (0.82 ± 0.10 folds, p = 0.0503, Fig. 4E and G), and cyclin D1 ($0.81 \pm$
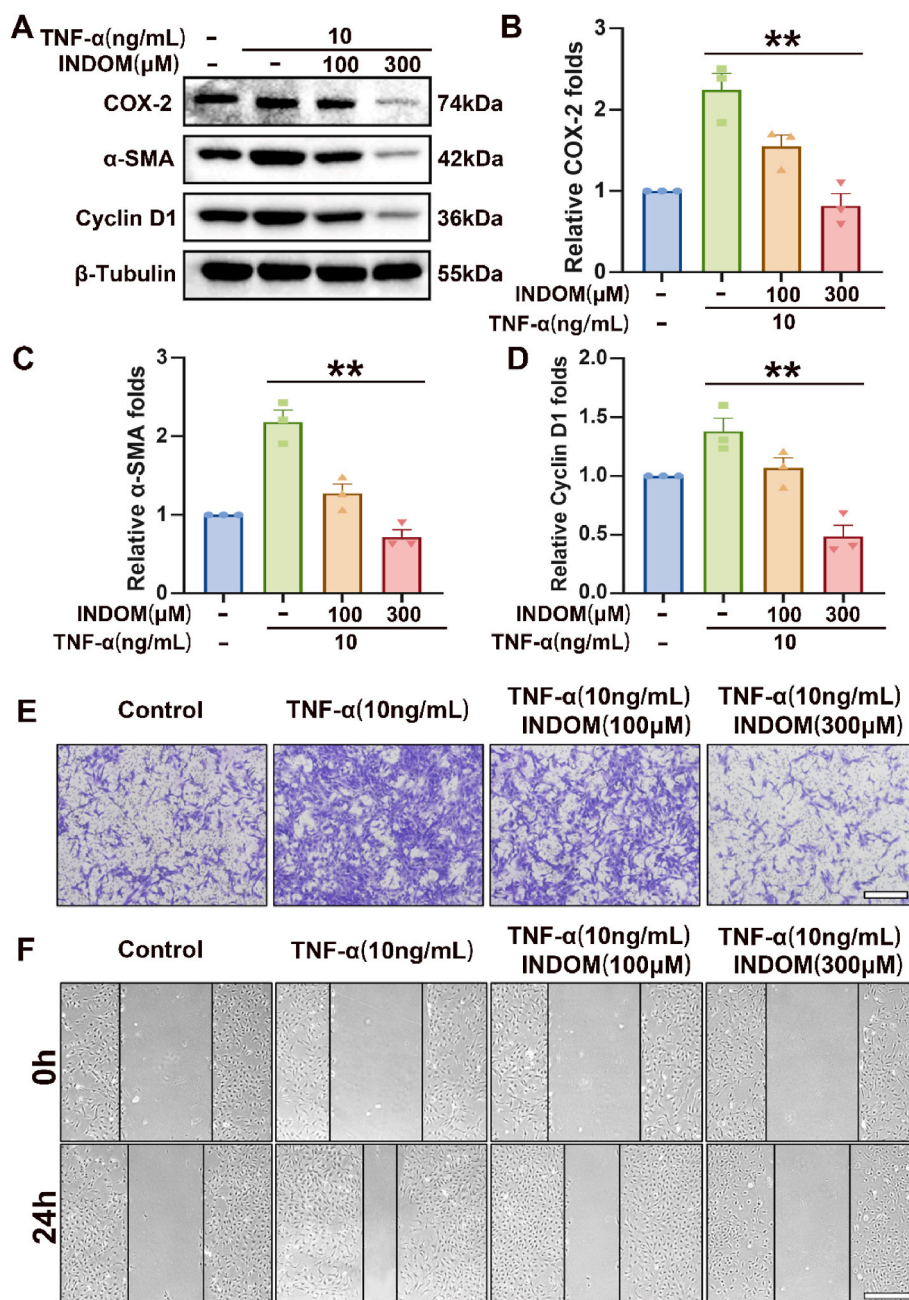
Fig. 2. Effects of INDOM on migration and EMT in lens epithelial cells. (A) Effects of INDOM in different concentrations on the TNF-α-activated up-regulation of COX-2, α-SMA, and cyclin D1 protein expression levels detected by Western blot. Quantification of COX-2 (B), α-SMA (C), and cyclin D1 (D) protein expression was shown above (**p < 0.01 between groups, n = 3). The transwell (E) and wound-healing results (F) showed the inhibitory effects of INDOM on TNF-α-activated cell migration (Scale bar, 500 μm).

0.10 folds, p = 0.313, Fig. 4E and H) between the P62 siRNA + TNF-α group and P62 siRNA + TNF-α + INDOM group, which indicated that the inhibitory effect of INDOM on EMT was significantly limited by P62 siRNA transfection.

Further, the immunofluorescence assay was performed to visualize the interaction between P62 and the transcription factor Snail. Immunofluorescent images showed that the fluorescence intensities of both P62 and Snail in the group treated with 10 ng/mL TNF-α remarkably increased compared with that of the control group, and their obvious co-localization was detected in the cytoplasm after TNF-α stimulation (Fig. 4F). Treatment with 300 μM INDOM significantly decreased the fluorescence intensities of both P62 and Snail compared with those in the group treated with TNF-α alone. To sum up, these results suggested that activation of autophagy could suppress TNF-α-stimulated EMT in LECs, and the regulation of Snail by P62 is critical in this process.

3.5. PCO prophylaxis experiments in vivo

The rabbit PCO model was established to evaluate the effects of INDOM-IOLs *in vivo*. The slit-lamp system was used to assess the PCO and anterior chamber inflammations at 3 days, 7 days, 14 days, and 42 days after phacoemulsification and IOL implantation surgery. As shown in Fig. 5B and C, both short-term postoperative inflammation and long-term PCO development were significantly reduced in the INDOM-IOL group compared with the Ctrl-IOL group and PLGA-IOL group. Intriguingly, the PCO development in the INDOM drops group was not effectively controlled. The PCO of the Ctrl-IOL, PLGA-IOL, and INDOM drops groups could be detected at 14 days post-operation. The gradings of PCO at 42 days were shown in Fig. 5E. The mean grading of the INDOM-IOL group was 1.20 ± 0.34, significantly lower than that of the Ctrl-IOL group (3.10 ± 0.36), PLGA-IOL group (3.00 ± 0.32), and INDOM drops group (2.60 ± 0.29). The Miyake-Apple images provided a more intuitively clear view of the posterior capsule in each group, which
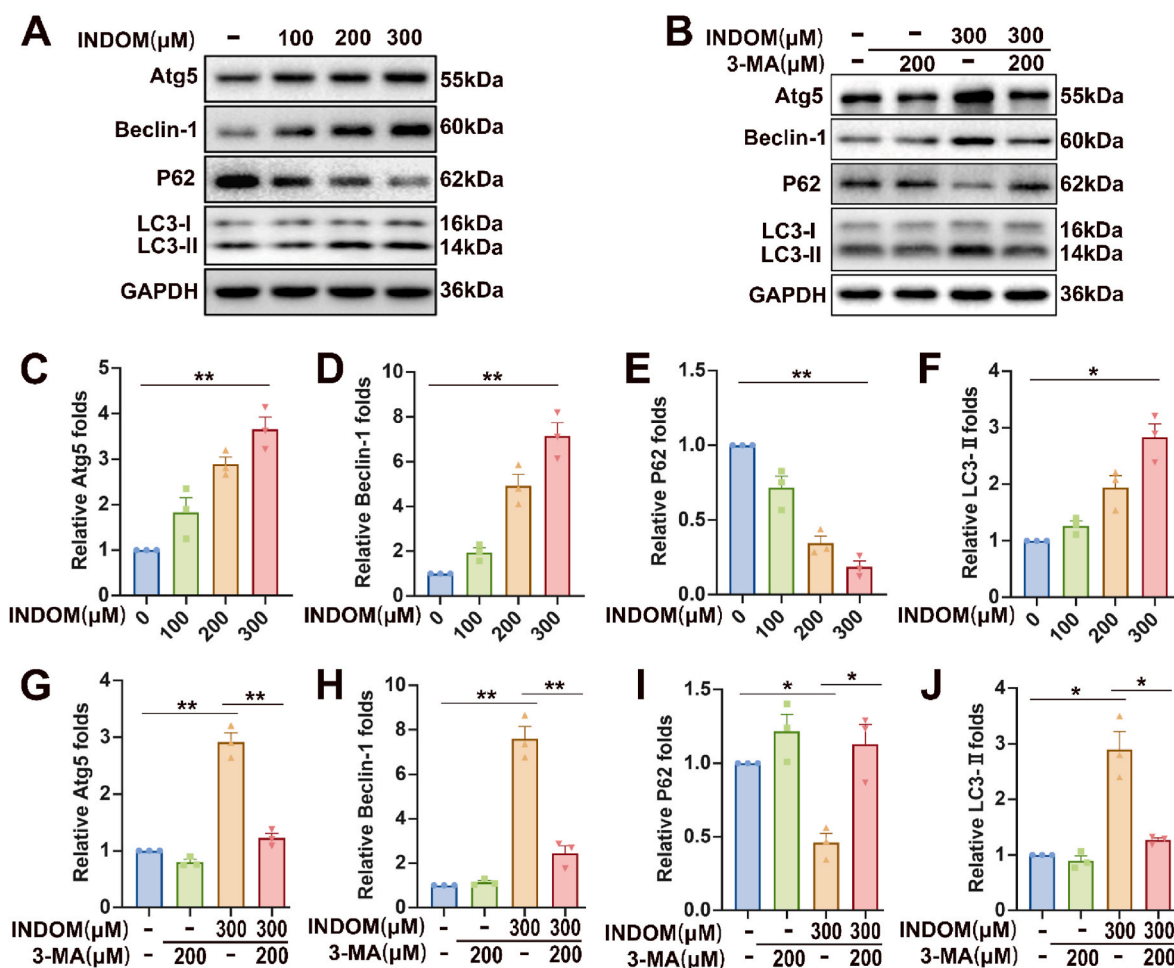
Fig. 3. Effects of INDOM on autophagy-related proteins in LECs. (A) Effects of INDOM in different concentrations on expression levels of Atg5, Beclin-1, P62, and LC3-I/II detected by Western blot. (B) Effects of 3-MA on INDOM-activated expression levels of Atg5, Beclin-1, P62, and LC3-I/II detected by Western blot. Quantification of Atg5 (C), Beclin-1 (D), P62 (E), and LC3-I/II (F) protein expression was shown above (*$p < 0.05$, **$p < 0.01$ between groups, $n = 3$). Quantification of Atg5 (G), Beclin-1 (H), P62 (I), and LC3-I/II (J) protein expression was shown above (*$p < 0.05$, **$p < 0.01$ between groups, $n = 3$).

showed that the posterior capsules were still extremely smooth and transparent in the INDOM-IOL group; meanwhile, the posterior capsules of Ctrl-IOL, PLGA-IOL, and INDOM drops groups were accumulated with lots of proliferative and fibrous materials (Fig. 5D). Furthermore, histological and immunofluorescence images showed no accumulated cells and proliferative layers in posterior capsules, especially in the central zone, of the INDOM-IOL group (Fig. 5D). However, a large number of cells, stained with tubulin and F-actin, were detected in the posterior capsules of the Ctrl-IOL, PLGA-IOL, and INDOM drops groups (Fig. 5F). These results revealed that the novel INDOM-IOL exhibited an excellent effect on PCO prophylaxis in the rabbit model.

Of note, after the inflammation of the anterior chamber subsided by 14 days postoperatively, the morphology and characteristics of the posterior capsule could be clearly observed through the novel INDOM-IOL, which indicated that INDOM-IOL maintained excellent transmittance in vivo (Fig. 5B and C).

3.6. Cytotoxicity assessments in vitro and vivo

To confirm the biosafety of INDOM, the cell viability test was verified by CCK-8 assay with three human ocular tissue-derived cell lines, including HCEC, ARPE-19, and HLEC-B3 [42,43]. The results showed that the cell viability of the three cell lines was all above 80% after exposure to 500 μM INDOM (Fig. 6A, B, and 6C). In addition, a live/dead cell (calcein-AM/PI) test was performed in HLEC-B3, and the results

showed that the vast majority of cells were stained with green fluorescence, and few cells were stained red after exposure to INDOM, which is consistent with the CCK-8 results (Fig. 6D). Collectively, these results demonstrated the low cytotoxicity and safety of INDOM in vitro.

In vivo, the rabbits were sacrificed by overdose anesthesia 42 days after surgery, and the H&E staining was performed to observed the ocular tissues. No obvious abnormality was found in the ocular tissues, including corneas, irises, and retinas, of all the groups (Figs. 5D and 6E). The cornea and retina of all animals were structurally intact and well-defined without edema and inflammatory cell infiltration. All animals had no abnormal performance during the whole experiment. Therefore, a conclusion can be drawn that the novel INDOM-IOL has good safety and biocompatibility while exerting the effect on PCO prophylaxis in vivo.

4. Discussion

PCO is a severe long-term complication after cataract surgery, and the pathogenesis has not been fully revealed yet [44]. The redesign and surface modification of IOLs is a vital topic in PCO prevention recently [45,46]. The redesign of IOLs is mainly to modify the IOLs into sharper square-edged ones, which can act as a physical barrier in the capsular bag to prevent the LECs from migrating toward the posterior capsule. Therefore, the sharp square-edged IOLs with barrier effect were used in the present study. Previous studies argued that IOLs could be assembled
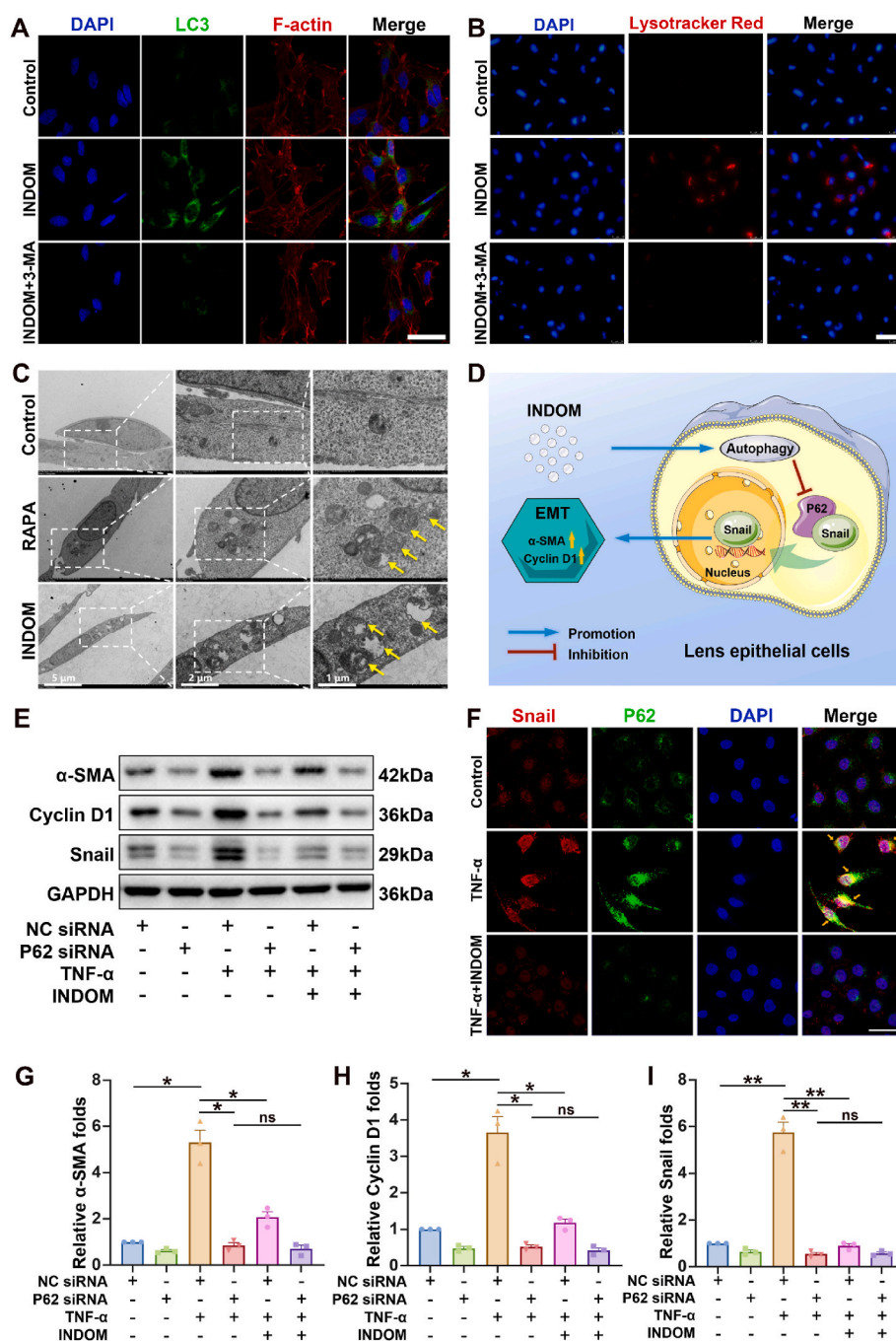
Fig. 4. INDOM regulates EMT by activating autophagy in LECs. (A) Immunofluorescence assay exhibited the effects of INDOM on the activation of autophagy in LECs. The number of LC3 stained puncta (green) in LECs increased significantly in the group treated with 300 μM INDOM for 24 h; and 200 μM 3-MA inhibited the effect of INDOM (Scale bar, 100 μm). (B) Lysosomes were stained with Lysotracker Red in the group treated with 300 μM INDOM for 24 h (Scale bar, 100 μm). (C) TEM images showed that the number of autophagic vacuoles (AV, yellow arrows) was significantly increased in both the positive control rapamycin (RAPA, 1 μM) group and INDOM (300 μM) group compared with that in the control group (Scale bar, 5 μm, 2 μm, and 1 μm). (D) Schematic illustration of the mechanism of INDOM inhibiting EMT by activating autophagy in LECs. (E) The LECs were transfected with P62 siRNA or NC siRNA, and treated with or without 300 μM INDOM and 10 ng/mL TNF-α. The expression levels of Snail, cyclin D1, and α-SMA was detected by Western blot. Quantification of α-SMA (G), cyclin D1 (H), and Snail (I) protein expression was shown above (*p < 0.05, **p < 0.01 between groups, ns represents no significance, n = 3). (F) Immunofluorescence staining of P62 (green) and Snail (red) in LECs was detected after treatment with or without 300 μM INDOM and 10 ng/mL TNF-α. The co-localization sites of P62 and Snail were marked by yellow arrows (Scale bar, 40 μm).

with anti-adhesion properties through surface modification to prevent the formation of PCO [10,45]. However, recent literature suggested that residual lens epithelial cells tend to proliferate on the native capsule rather than on the surface of IOL, that is, IOL materials are hardly able to enhance the barrier effect of IOLs through its bioactive properties, and the anti-adhesion properties of IOL materials may have minimal impact on PCO prevention [47]. Pharmacological intervention against PCO may be a better alternative.

INDOM is a commonly used anti-inflammatory drug. Interestingly, our study demonstrated its effect on the activation of autophagy in LECs. Autophagy plays a vital role in tissue development and cell homeostasis maintenance [48–50]. Previous studies found that several lens diseases, such as age-related cataracts, congenital cataracts, and diabetic cataracts, are associated with abnormal autophagy regulation [51,52]. In terms of PCO, Chandler et al. reported that cyclosporine A could activate

the autophagy-mediated cell death ex *vivo* [26]. Liu et al. also found that sulforaphane could promote endoplasmic reticulum (ER) stress and autophagy through reactive oxygen species (ROS) stimulation to inhibit cell growth in the human lens capsular bag model [53]. In this study, we found that INDOM significantly up-regulated autophagy-related proteins, including Atg5, Beclin-1, and LC3-I/II, which could be inhibited by the established autophagy inhibitor 3-MA, illustrating that INDOM was capable of stimulating the activation of autophagy in LECs. Of note, INDOM also inhibited the expression of P62. Meanwhile, we also verified that INDOM could inhibit the over-expression of EMT markers triggered by TNF-α in LECs. A recent study reported that, in the high glucose-induced EMT of LECs, P62 has a positive regulatory effect on Snail, which was identified as a key moderator in the EMT process [41]. In addition, the inhibition of autophagy induced the EMT of alveolar epithelial cells, which would contribute to augmenting local
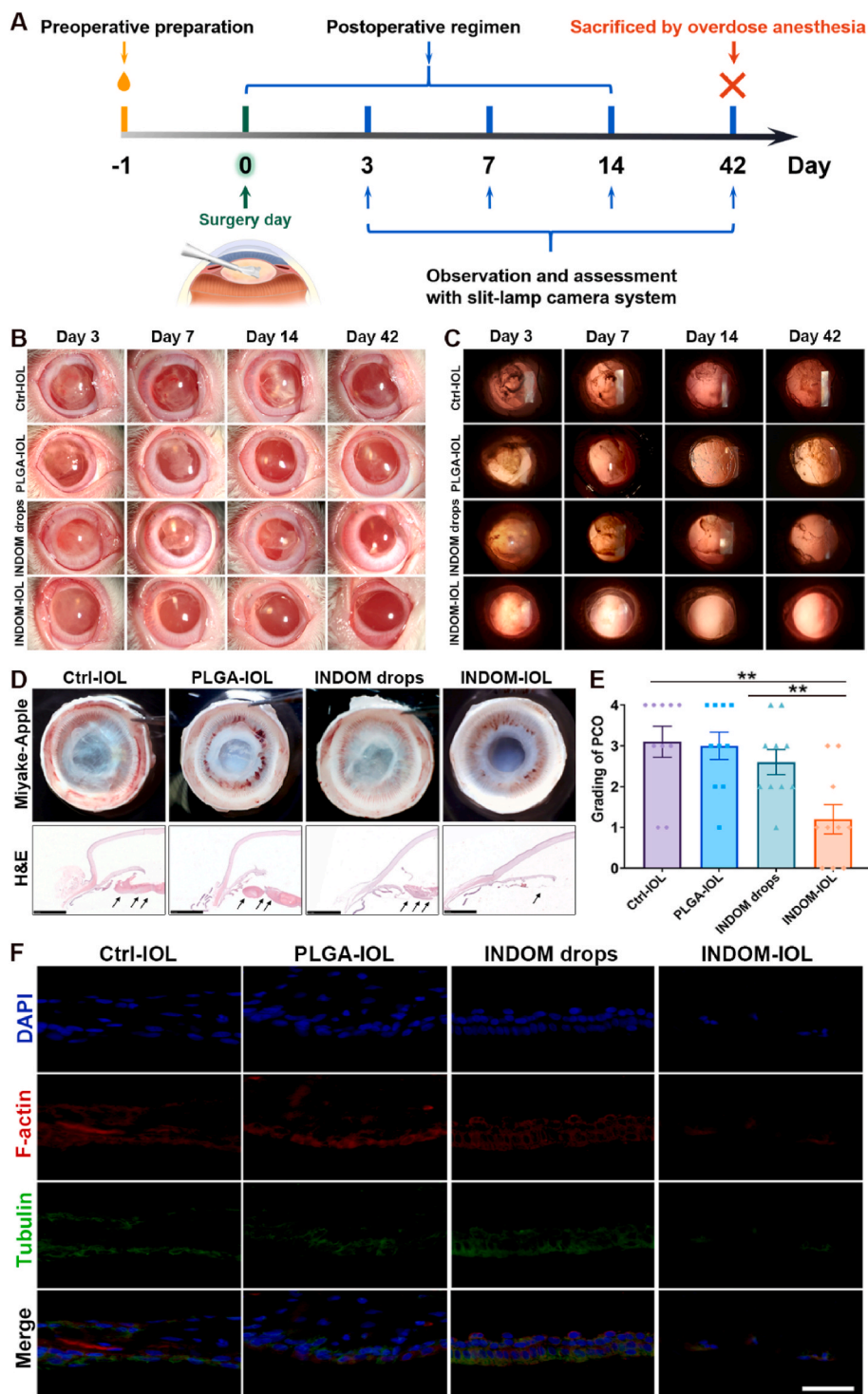
Fig. 5. Effect of INDOM-IOLs on PCO prophylaxis in rabbit PCO model: (A) Scheme of rabbit PCO model establishment and treatment. (B) Slit-lamp system was used to assess anterior chamber at 3 days, 7 days, 14 days, and 42 days postoperatively. (C) Slit-lamp system was used to assess posterior capsules at 3 days, 7 days, 14 days, and 42 days postoperatively. (D) Miyake-Apple view images of the posterior capsule and the hematoxylin and eosin (H&E) staining of the whole anterior segment structures in each group. Black arrows showed that no accumulation of proliferative layers in posterior capsules of the INDOM-IOL group, while many proliferative materials detected in the posterior capsules of the Ctrl-IOL, PLGA-IOL, and INDOM drops groups (Scale bar, 2.5 mm). (E) Grading of PCO formation in each group (**p < 0.01 between groups, n = 10). (F) Immunofluorescence assay of posterior capsule stained with tubulin (green) and F-actin (red), which showed that there was no cell deposition in the posterior capsule only in the INDOM-IOL group (Scale bar, 50 μm).

myofibroblast differentiation in pulmonary fibrosis [54]. The transcription factors for EMT might be protected in a P62-dependent manner, leading to the augmentation of EMT and migration in hepatocytes [55]. Therefore, we inferred that the activation of autophagy by INDOM might promote the inhibition of EMT in LECs, and P62 was likely to be the functional link between EMT and autophagy. Notably, impaired autophagy is involved in the pathogenesis of several fibrotic diseases, such as hepatic fibrosis, idiopathic pulmonary fibrosis and kidney fibrosis, and it is reported that autophagy activation can inhibit cell proliferation, EMT and fibrosis by suppressing tissue damage, chronic inflammation, DNA damage, and abnormal mitosis, rather than directly leading to cell death [56–61]. Therefore, as a fibrotic disease, it is inferred that autophagy may also play a similar role in the process of PCO, and INDOM is able to inhibit the EMT and fibrosis of pathological LECs, but has no direct leading to healthy cell death in other intraocular tissues. Furthermore, we revealed that activation of autophagy could suppress EMT *via* interaction of P62 and Snail in LECs, and INDOM could regulate the expression of the transcription factor Snail to suppress EMT by repressing P62 expression upon activation of autophagy. Significantly, autophagy was demonstrated to be a potential therapeutic target for the down-regulation of EMT in LECs.

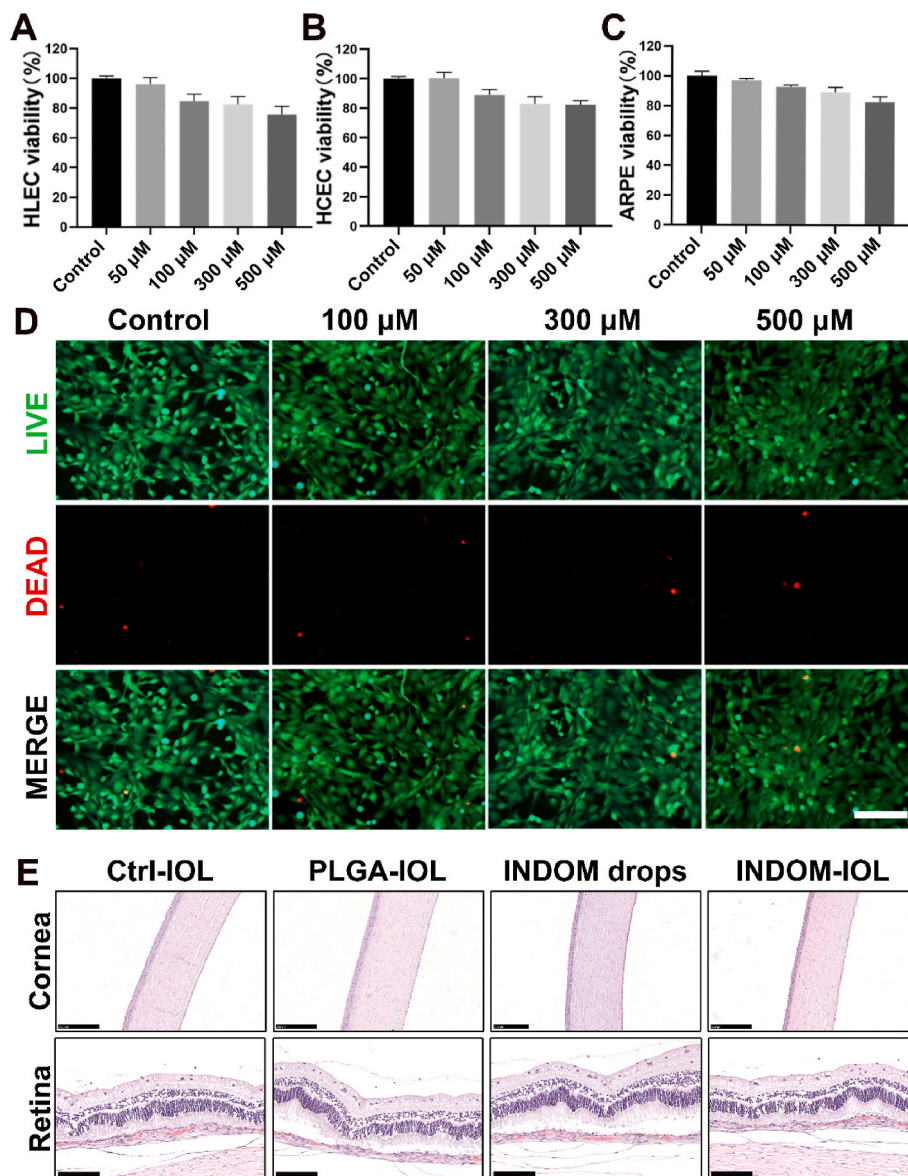Optimized IOL combined with appropriate drug intervention can

Fig. 6. Cytotoxicity assessments. Cell viability of HLEC (A), HCEC (B), and ARPE-19 (C) exposed to different concentrations of INDOM (50 μM, 100 μM, 300 μM, and 500 μM) for 24 h. (D) Live/dead cell (calcein-AM/PI) test of the HCECs exposed to different concentrations of INDOM (100 μM, 300 μM, and 500 μM) for 24 h (Scale bar, 500 μm). (E) H&E staining of the corneas, and retinas in each group (Scale bar in cornea images, 250 μm; scale bar in retina images, 100 μm).

provide the best opportunity for PCO prevention. Previous studies have reported that hydrophobic IOLs have shown better PCO prevention because they adhere better to the posterior capsular bag, therefore, hydrophobic acrylic IOLs with plate haptics and sharp square-edge were involved in this study [12,47]. Encouraged by the results of *in vitro* experiments, we loaded INDOM on the plate haptics of IOLs with PLGA using ultrasonic spray technology. PLGA, approved by the Food and Drug Administration (FDA) for drug delivery system in clinic, provides the present IOL with excellent sustained drug release properties, which maintains a smooth release of INDOM for 42 days. The PLGA coating is firmly attached to the surface of IOL haptics and has excellent biocompatibility and biodegradability [62–64]. In animal experiments, the PLGA coating did not fall off during IOL implantation, even the IOLs completely folded through the corneal tunnel incisions. Most importantly, the INDOM-IOL exhibited excellent anti-inflammation and anti-PCO effects *in vivo*. In contrast, topical administration of INDOM had few anti-PCO effects. Regardless of the route of drug delivery, it is indispensable to deliver a constant and adequate drug dosage to the target tissues. As expected, this novel drug-eluting IOL achieved high

efficacy with low drug dosage.

5. Conclusion

The present study demonstrated the potential of INDOM as a pharmacological intervention for PCO prevention. INDOM could not only inhibit the migration and EMT triggered by TNF-α but also stimulate the activation of autophagy in LECs as autophagy was a potential therapeutic target for the down-regulation of EMT in LECs. Afterward, the INDOM-IOLs with optimized IOL structures and sustained drug release properties were developed for PCO prophylaxis. These novel INDOM-IOLs showed excellent anti-inflammatory and anti-PCO effects with high efficiency *in vivo*, thus providing a promising approach for PCO prophylaxis.

Ethic approval

All animal experiments were approved by the Laboratory Animal Ethics Committee of the Second Affiliated Hospital, School of Medicine,

Zhejiang University (approval No. 098/2022).

CRediT authorship contribution statement

Xiaobo Zhang: Writing – original draft, Conceptualization, Data curation, Formal analysis. **Jing Wang:** Data curation, Formal analysis, Methodology, Writing – review & editing. **Jingwei Xu:** Data curation, Formal analysis, Investigation, Writing – review & editing. **Wen Xu:** Writing – review & editing, Supervision. **Yin Zhang:** Data curation, Formal analysis, Visualization. **Chenqi Luo:** Data curation, Formal analysis, Software. **Shuang Ni:** Data curation, Formal analysis, Investigation. **Haijie Han:** Writing – review & editing, Data curation, Formal analysis. **Xingchao Shentu:** Data curation, Formal analysis. **Juan Ye:** Data curation, Formal analysis. **Jian Ji:** Writing – review & editing, Supervision. **Ke Yao:** Writing – review & editing, Supervision.

Declarations of competing interest

The authors declare that they have no financial and personal relationships with other people or organizations that could have appeared to influence the work reported in this paper.

Acknowledgments

References

[1] Y.-C. Liu, M. Wilkins, T. Kim, B. Malyugin, J.S. Mehta, Cataracts, Lancet 390 (2017) 600–612, https://doi.org/10.1016/S0140-6736(17)30544-5.
[2] A.C. Day, J.M. Burr, K. Bennett, C. Bunce, C.J. Doré, G.S. Rubin, et al., Femtosecond laser-assisted cataract surgery versus phacoemulsification cataract surgery (FACT): a randomized noninferiority trial, Ophthalmology 127 (2020) 1012–1019, https://doi.org/10.1016/j.ophtha.2020.02.028.
[3] M. Lei, Z. Peng, Q. Dong, Y. He, Z. Zhang, X. Zhang, et al., A novel capsular tension ring as local sustained-release carrier for preventing posterior capsule opacification, Biomaterials 89 (2016) 148–156, https://doi.org/10.1016/j.biomaterials.2016.02.038.
[4] A. Taiyab, J. Holms, J.A. West-Mays, β-Catenin/Smad3 interaction regulates transforming growth factor-β-induced epithelial to mesenchymal transition in the lens, Int. J. Mol. Sci. 20 (2019) 2078, https://doi.org/10.3390/ijms20092078.
[5] Y. Seo, S. Kim, H.S. Lee, J. Park, K. Lee, I. Jun, et al., Femtosecond laser induced nano-textured micropatterning to regulate cell functions on implanted biomaterials, Acta Biomater. 116 (2020) 138–148, https://doi.org/10.1016/j.actbio.2020.08.044.
[6] J.D. Wesolosky, M. Tennant, C.J. Rudnisky, Rate of retinal tear and detachment after neodymium:YAG capsulotomy, J. Cataract Refract. Surg. 43 (2017) 923–928, https://doi.org/10.1016/j.jcrs.2017.03.046.
[7] J.M. Lindholm, I. Laine, R. Tuuminen, Five-Year cumulative incidence and risk factors of Nd:YAG capsulotomy in 10 044 hydrophobic acrylic 1-piece and 3-piece intraocular lenses, Am. J. Ophthalmol. 200 (2019) 218–223, https://doi.org/10.1016/j.ajo.2019.01.010.
[8] G. Cooksley, J. Lacey, M.K. Dymond, S. Sandeman, Factors affecting posterior capsule opacification in the development of intraocular lens materials, Pharmaceutics 13 (2021) 860, https://doi.org/10.3390/pharmaceutics13060860.
[9] E.M. Krall, E.M. Arlt, G. Jell, C. Strohmaier, S. Moussa, A.K. Dexl, Prospective randomized intraindividual comparison of posterior capsule opacification after implantation of an IOL with and without heparin surface modification, J. Refract. Surg. 31 (2015) 466–472, https://doi.org/10.3928/1081597x-20150623-05.
[10] Y. Han, J. Tang, J. Xia, R. Wang, C. Qin, S. Liu, et al., Anti-adhesive and antiproliferative synergistic surface modification of intraocular lens for reduced posterior capsular opacification, Int. J. Nanomed. 14 (2019) 9047–9061, https://doi.org/10.2147/ijn.S215802.
[11] X. Huang, C. Luo, L. Lin, L. Zhang, H. Li, K. Yao, et al., UV-assisted treatment on hydrophobic acrylic IOLs anterior surface with methacryloyloxyethyl phosphorylcholine: reducing inflammation and maintaining low posterior capsular opacification properties, Mater. Sci. Eng. C Mater. Biol. Appl. 75 (2017) 1289–1298, https://doi.org/10.1016/j.msec.2017.03.029.

[12] A. Topete, J. Tang, X. Ding, H.P. Filipe, J.A. Saraiva, A.P. Serro, et al., Dual drug delivery from hydrophobic and hydrophilic intraocular lenses: in-vitro and in-vivo studies, J. Contr. Release 326 (2020) 245–255, https://doi.org/10.1016/j.jconrel.2020.07.020.
[13] K. Ongkasin, Y. Masmoudi, C.M. Wertheimer, A. Hillenmayer, K.H. Eibl-Lindner, E. Badens, Supercritical fluid technology for the development of innovative ophthalmic medical devices: drug loaded intraocular lenses to mitigate posterior capsule opacification, Eur. J. Pharm. Biopharm. 149 (2020) 248–256, https://doi.org/10.1016/j.ejpb.2020.02.011.
[14] C. Qin, S. Liu, S. Wen, Y. Han, S. Chen, J. Qie, et al., Enhanced PCO prevention of drug eluting IOLs via endocytosis and autophagy effects of a PAMAM dendrimer, J. Mater. Chem. B 9 (2021) 793–800, https://doi.org/10.1039/d0tb02530e.
[15] D.S. Borkar, M.E. Lacouture, S. Basti, Spectrum of ocular toxicities from epidermal growth factor receptor inhibitors and their intermediate-term follow-up: a five-year review, Support. Care Cancer 21 (2013) 1167–1174, https://doi.org/10.1007/s00520-012-1645-y.
[16] M.H. Nam, A.J.O. Smith, M.B. Pantcheva, K.U. Park, J.A. Brzezinski, J.J. Galligan, et al., Aspirin inhibits TGFβ2-induced epithelial to mesenchymal transition of lens epithelial cells: selective acetylation of K56 and K122 in histone H3, Biochem. J. 477 (2020) 75–97, https://doi.org/10.1042/bcj20190540.
[17] J. Tang, S. Liu, Y. Han, R. Wang, J. Xia, H. Chen, et al., Surface modification of intraocular lenses via photodynamic coating for safe and effective PCO prevention, J. Mater. Chem. B 9 (2021) 1546–1556, https://doi.org/10.1039/d0tb02802a.
[18] E. Kubo, T. Shibata, D.P. Singh, H. Sasaki, Roles of TGF β and FGF signals in the lens: tropomyosin regulation for posterior capsule opacity, Int. J. Mol. Sci. 19 (2018) 3093, https://doi.org/10.3390/ijms19103093.
[19] B. Ma, R. Jing, J. Liu, L. Yang, J. Li, L. Qin, et al., CTGF contributes to the development of posterior capsule opacification: an in vitro and in vivo study, Int. J. Biol. Sci. 14 (2018) 437–448, https://doi.org/10.7150/ijbs.23946.
[20] A. Sauer, T. Bourcier, D. Gaucher, E. Candolfi, C. Speeg-Schatz, Intraocular cytokines imbalance in congenital cataract and its impact on posterior capsule opacification, Graefes Arch. Clin. Exp. Ophthalmol. 254 (2016) 1013–1018, https://doi.org/10.1007/s00417-016-3313-2.
[21] N. Dong, X. Tang, B. Xu, miRNA-181a inhibits the proliferation, migration, and epithelial-mesenchymal transition of lens epithelial cells, Invest. Ophthalmol. Vis. Sci. 56 (2015) 993–1001, https://doi.org/10.1167/iovs.14-15860.
[22] N. Mizushima, M. Komatsu, Autophagy: renovation of cells and tissues, Cell 147 (2011) 728–741, https://doi.org/10.1016/j.cell.2011.10.026.
[23] G.R. De Meyer, M.O. Grootaert, C.F. Michiels, A. Kurdi, D.M. Schrijvers, W. Martinet, Autophagy in vascular disease, Circ. Res. 116 (2015) 468–479, https://doi.org/10.1161/circresaha.116.303804.
[24] Y. Deng, P. Song, X. Chen, Y. Huang, L. Hong, Q. Jin, et al., 3-Bromopyruvate-Conjugated nanoplatform-induced pro-death autophagy for enhanced photodynamic therapy against hypoxic tumor, ACS Nano 14 (2020) 9711–9727, https://doi.org/10.1021/acsnano.0c01350.
[25] A. Burhop, S. Bag, M. Grigalunas, S. Woitalla, P. Bodenbinder, L. Brieger, et al., Synthesis of indofulvin pseudo-natural products yields a new autophagy inhibitor chemotype, Adv. Sci. 8 (2021), 2102042, https://doi.org/10.1002/advs.202102042.
[26] H.L. Chandler, K.J. Gervais, E.A. Lutz, E.M. Curto, R.B. Matusow, D.A. Wilkie, et al., Cyclosporine A prevents ex vivo PCO formation through induction of autophagy-mediated cell death, Exp. Eye Res. 134 (2015) 63–72, https://doi.org/10.1016/j.exer.2015.03.020.
[27] H. Feng, Z. Yang, X. Bai, M. Yang, Y. Fang, X. Zhang, et al., Therapeutic potential of a dual mTORC1/2 inhibitor for the prevention of posterior capsule opacification: an in vitro study, Int. J. Mol. Med. 41 (2018) 2099–2107, https://doi.org/10.3892/ijmm.2018.3398.
[28] A.L. Lovering, J.P. Ride, C.M. Bunce, J.C. Desmond, S.M. Cummings, S.A. White, Crystal structures of prostaglandin D(2) 11-ketoreductase (AKR1C3) in complex with the nonsteroidal anti-inflammatory drugs flufenamic acid and indomethacin, Cancer Res. 64 (2004) 1802–1810, https://doi.org/10.1158/0008-5472.can-03-2847.
[29] A. Ikeda, E. Funakoshi, M. Araki, B. Ma, Y. Karuo, A. Tarui, et al., Structural modification of indomethacin toward selective inhibition of COX-2 with a significant increase in van der Waals contributions, Bioorg. Med. Chem. 27 (2019) 1789–1794, https://doi.org/10.1016/j.bmc.2019.03.021.
[30] L. Friedrich, G. Cingolani, Y.-H. Ko, M. Iaselli, M. Miciaccia, M.G. Perrone, et al., Learning from nature: from a marine natural product to synthetic cyclooxygenase-1 inhibitors by automated de novo design, Adv. Sci. 8 (2021), 2100832, https://doi.org/10.1002/advs.202100832.
[31] C.Y. Ock, J.M. Park, Y.M. Han, M. Jeong, M.Y. Kim, H.J. Lee, et al., Genetic ablation or pharmacologic inhibition of autophagy mitigated NSAID-associated gastric damages, J. Mol. Med. (Berl.) 95 (2017) 405–416, https://doi.org/10.1007/s00109-016-1491-3.
[32] S.M. Gebril, Y. Ito, M.A. Shibata, K. Maemura, E.E. Abu-Dief, M.R.A. Hussein, et al., Indomethacin can induce cell death in rat gastric parietal cells through alteration of some apoptosis- and autophagy-associated molecules, Int. J. Exp. Pathol. 101 (2020) 230–247, https://doi.org/10.1111/iep.12370.
[33] U.B. Kompella, R.R. Hartman, M.A. Patil, Extraocular, periocular, and intraocular routes for sustained drug delivery for glaucoma, Prog. Retin. Eye Res. (2020), 100901, https://doi.org/10.1016/j.preteyeres.2020.100901.
[34] W. Fan, H. Han, Y. Chen, X. Zhang, Y. Gao, S. Li, et al., Antimicrobial nanomedicine for ocular bacterial and fungal infection, Drug Deliv. Transl. Res. 11 (2021) 1352–1375, https://doi.org/10.1007/s13346-021-00966-x.
[35] J. Wang, H.L. Qian, S.Y. Chen, W.P. Huang, D.N. Huang, H.Y. Hao, et al., miR-22 eluting cardiovascular stent based on a self-healable spongy coating inhibits in-

stent restenosis, Bioact. Mater. 6 (2021) 4686–4696, https://doi.org/10.1016/j.bioactmat.2021.04.037.

[36] J. Wang, X.-C. Chen, Y.-F. Xue, M. Hu, Y.-B. Wang, K.-F. Ren, et al., Thermo-triggered ultrafast self-healing of microporous coating for on-demand encapsulation of biomacromolecules, Biomaterials 192 (2019) 15–25, https://doi.org/10.1016/j.biomaterials.2018.10.038.

[37] L.G. Vargas, A.M. Izak, D.J. Apple, L. Werner, S.K. Pandey, R.H. Trivedi, Implantation of a single-piece, hydrophilic, acrylic, minus-power foldable posterior chamber intraocular lens in a rabbit model: clinicopathologic study of posterior capsule opacification, J. Cataract Refract. Surg. 29 (2003) 1613–1620, https://doi.org/10.1016/s0886-3350(03)00215-3.

[38] X. Zhang, K. Lai, S. Li, J. Wang, J. Li, W. Wang, et al., Drug-eluting intraocular lens with sustained bromfenac release for conquering posterior capsular opacification, Bioact. Mater. 9 (2022) 343–357, https://doi.org/10.1016/j.bioactmat.2021.07.015.

[39] Y. Ma, W. Zhao, Y. Li, Y. Pan, S. Wang, Y. Zhu, et al., Structural optimization and additional targets identification of antisense oligonucleotide G3139 encapsulated in a neutral cytidinyl-lipid combined with a cationic lipid in vitro and in vivo, Biomaterials 197 (2019) 182–193, https://doi.org/10.1016/j.biomaterials.2018.12.033.

[40] B. Zhitomirsky, H. Farber, Y.G. Assaraf, LysoTracker and MitoTracker Red are transport substrates of P-glycoprotein: implications for anticancer drug design evading multidrug resistance, J. Cell Mol. Med. 22 (2018) 2131–2141, https://doi.org/10.1111/jcmm.13485.

[41] J. Li, W. Ye, W. Xu, T. Chang, L. Zhang, J. Ma, et al., Activation of autophagy inhibits epithelial to mesenchymal transition process of human lens epithelial cells induced by high glucose conditions, Cell. Signal. 75 (2020), 109768, https://doi.org/10.1016/j.cellsig.2020.109768.

[42] S. Li, Z. Lu, Y. Huang, Y. Wang, Q. Jin, X. Shentu, et al., Anti-oxidative and anti-inflammatory micelles: break the dry eye vicious cycle, Adv. Sci. 9 (2022), 2200435, https://doi.org/10.1002/advs.202200435.

[43] H. Han, Y. Gao, M. Chai, X. Zhang, S. Liu, Y. Huang, et al., Biofilm microenvironment activated supramolecular nanoparticles for enhanced photodynamic therapy of bacterial keratitis, J. Contr. Release 327 (2020) 676–687, https://doi.org/10.1016/j.jconrel.2020.09.014.

[44] H. Lin, H. Ouyang, J. Zhu, S. Huang, Z. Liu, S. Chen, et al., Lens regeneration using endogenous stem cells with gain of visual function, Nature 531 (2016) 323–328, https://doi.org/10.1038/nature17181.

[45] Q. Lin, J. Tang, Y. Han, X. Xu, X. Hao, H. Chen, Hydrophilic modification of intraocular lens via surface initiated reversible addition-fragmentation chain transfer polymerization for reduced posterior capsular opacification, Colloids Surf. B Biointerfaces 151 (2017) 271–279, https://doi.org/10.1016/j.colsurfb.2016.12.028.

[46] A.P. Vieira, A.F.R. Pimenta, D. Silva, M.H. Gil, P. Alves, P. Coimbra, et al., Surface modification of an intraocular lens material by plasma-assisted grafting with 2-hydroxyethyl methacrylate (HEMA), for controlled release of moxifloxacin, Eur. J. Pharm. Biopharm. 120 (2017) 52–62, https://doi.org/10.1016/j.ejpb.2017.08.006.

[47] J.A. Eldred, J. Zheng, S. Chen, I.M. Wormstone, An in vitro human lens capsular bag model adopting a graded culture regime to assess putative impact of IOLs on PCO formation, Invest. Ophthalmol. Vis. Sci. 60 (2019) 113–122, https://doi.org/10.1167/iovs.18-25930.

[48] A.N. Hale, D.J. Ledbetter, T.R. Gawriluk, E.B. Rucker 3rd, Autophagy: regulation and role in development, Autophagy 9 (2013) 951–972, https://doi.org/10.4161/auto.24273.

[49] H. Zhang, Y. Ren, L. Hou, J. Chang, Z. Zhang, H. Zhang, Positioning remodeling nanogels mediated codelivery of antivascular drug and autophagy inhibitor for cooperative tumor therapy, ACS Appl. Mater. Interfaces 12 (2020) 6978–6990, https://doi.org/10.1021/acsami.9b22412.

[50] K.M. Dhanabalan, A.A. Dravid, S. Agarwal, R.K. Sharath, A.K. Padmanabhan, R. Agarwal, Intra-articular injection of rapamycin microparticles prevent senescence and effectively treat osteoarthritis, Bioeng. Transl. Med. (2022), e10298, https://doi.org/10.1002/btm2.10298.

[51] X. Ping, J. Liang, K. Shi, J. Bao, J. Wu, X. Yu, et al., Rapamycin relieves the cataract caused by ablation of Gja8b through stimulating autophagy in zebrafish, Autophagy (2021) 1–15, https://doi.org/10.1080/15548627.2021.1872188.

[52] H. Morishita, S. Eguchi, H. Kimura, J. Sasaki, Y. Sakamaki, M.L. Robinson, et al., Deletion of autophagy-related 5 (Atg5) and Pik3c3 genes in the lens causes cataract independent of programmed organelle degradation, J. Biol. Chem. 288 (2013) 11436–11447, https://doi.org/10.1074/jbc.M112.437103.

[53] H. Liu, A.J. Smith, S.S. Ball, Y. Bao, R.P. Bowater, N. Wang, et al., Sulforaphane promotes ER stress, autophagy, and cell death: implications for cataract surgery, J. Mol. Med. (Berl.) 95 (2017) 553–564, https://doi.org/10.1007/s00109-016-1502-4.

[54] C. Hill, J. Li, D. Liu, F. Conforti, C.J. Brereton, L. Yao, et al., Autophagy inhibition-mediated epithelial-mesenchymal transition augments local myofibroblast differentiation in pulmonary fibrosis, Cell Death Dis. 10 (2019) 591, https://doi.org/10.1038/s41419-019-1820-x.

[55] G. Grassi, G. Di Caprio, L. Santangelo, G.M. Fimia, A.M. Cozzolino, M. Komatsu, et al., Autophagy regulates hepatocyte identity and epithelial-to-mesenchymal and mesenchymal-to-epithelial transitions promoting Snail degradation, Cell Death Dis. 6 (2015), e1880, https://doi.org/10.1038/cddis.2015.149.

[56] J.M. Pinkston, D. Garigan, M. Hansen, C. Kenyon, Mutations that increase the life span of C. elegans inhibit tumor growth, Science 313 (2006) 971–975, https://doi.org/10.1126/science.1121908.

[57] R. Mathew, V. Karantza-Wadsworth, E. White, Role of autophagy in cancer, Nat. Rev. Cancer 7 (2007) 961–967, https://doi.org/10.1038/nrc2254.

[58] A. Takamura, M. Komatsu, T. Hara, A. Sakamoto, C. Kishi, S. Waguri, et al., Autophagy-deficient mice develop multiple liver tumors, Genes Dev. 25 (2011) 795–800, https://doi.org/10.1101/gad.2016211.

[59] Y. Takagaki, S.M. Lee, Z. Dongqing, M. Kitada, K. Kanasaki, D. Koya, Endothelial autophagy deficiency induces IL6 - dependent endothelial mesenchymal transition and organ fibrosis, Autophagy 16 (2020) 1905–1914, https://doi.org/10.1080/15548627.2020.1713641.

[60] Y. Tian, J. Lv, Z. Su, T. Wu, X. Li, X. Hu, et al., LRRK2 plays essential roles in maintaining lung homeostasis and preventing the development of pulmonary fibrosis, Proc. Natl. Acad. Sci. U. S. A. 118 (2021), https://doi.org/10.1073/pnas.2106685118.

[61] J. Gao, B. Wei, T.M. de Assuncao, Z. Liu, X. Hu, S. Ibrahim, et al., Hepatic stellate cell autophagy inhibits extracellular vesicle release to attenuate liver fibrosis, J. Hepatol. 73 (2020) 1144–1154, https://doi.org/10.1016/j.jhep.2020.04.044.

[62] K. Park, Tolerance levels of PLGA microspheres in the eyes, J. Contr. Release 266 (2017) 365, https://doi.org/10.1016/j.jconrel.2017.11.010.

[63] Y. Zhang, H.F. Chan, K.W. Leong, Advanced materials and processing for drug delivery: the past and the future, Adv. Drug Deliv. Rev. 65 (2013) 104–120, https://doi.org/10.1016/j.addr.2012.10.003.

[64] R. Sheshala, G.C. Hong, W.P. Yee, V.S. Meka, R.R.S. Thakur, In situ forming phase-inversion implants for sustained ocular delivery of triamcinolone acetonide, Drug Del. Transl. Res. 9 (2019) 534–542, https://doi.org/10.1007/s13346-018-0491-y.